SCIENTIFIC REPORTS

OPEN

Magnetic character of holmium atom adsorbed on platinum surface

A. B. Shick[1], D. S. Shapiro[2,3], J. Kolorenc[1] & A. I. Lichtenstein[4]

Received: 21 December 2016
Accepted: 19 April 2017
Published online: 05 June 2017

We address a recent controversy concerning the magnetic state of holmium adatom on platinum surface. Within a combination of the density functional theory (DFT) with the exact diagonalization (ED) of Anderson impurity model, the $\langle J_z \rangle = 0$ paramagnetic ground state $|J = 8, J_z = \pm 8\rangle$ is found. In an external magnetic field, this state is transformed to a spin-polarized state with $\langle J_z \rangle \approx 6.7$. We emphasize the role of 5*d*–4*f* interorbital exchange polarization in modification of the 4*f* shell energy spectrum.

The study of single magnetic rare-earth (RE) atoms adsorbed on metallic[1–3] and insulating[4] solid surfaces recently became a subject of intense research. These "single-atom" magnets serve as benchmarks in a quest for the ultimate size limit of magnetic information storage. The major advance of observing the magnetic remanence was recently reported for the Ho adatom on MgO substrate[4]. The stable magnetic quantum state of the adatom was found on the time scale of 1500 s at 10 K temperature.

There is an ongoing debate whether the magnetic moment on Ho atom on Pt(111) surface (Ho@Pt) can be stable on the long time scale. Recent inelastic electron tunneling spectroscopy (IETS) measurements[1] reported the moment lifetime up to 700 s below 1 K temperature, due to the single-ion magnetic anisotropy. However, the x-ray spectroscopy experiments[2] have shown that the ground state of Ho is magnetically unstable, with no magnetic remanence. Moreover, the newer IETS experimental data[3] did not see neither signatures of the spin-flip excitations nor spin-based telegraph noise for Ho atoms. This indicates that the 4*f* electrons do not contribute to the spin polarized tunneling processes in RE atoms on metals.

Theoretical calculations can shed light on the controversy concerning the magnetic state of Ho@Pt. The two $|J = 8, J_z = \pm 8\rangle$ magnetic ground states pointing into and out of the Pt(111) surface were inferred from *ab initio* density functional theory (DFT) calculations[1]. The multiplet calculations[2] with the parameters chosen to reproduce the x-ray magnetic circular dichroism (XMCD) spectra resulted in $|J = 8, J_z = \pm 6\rangle$ ground states. Further analysis[5] critically reexamined the XMCD data analysis[2], and confirmed qualitatively the magnetically unstable ground state of Ho.

Up to date, conventional DFT and DFT+Coulomb U[6,7] (DFT+U) methodologies were used in the calculations of Ho@Pt[1,3]. Their main role was to identify the most favorable adsorption site and the optimal height for the Ho adatom above the Pt surface layer. While DFT+U can describe the chemical inertness of the 4*f* shell, it does not include the atomic multiplet effects, and can yield ambiguous results for the magnetic moments, or valence stability[8]. Recently, the combination of DFT with the dynamical mean field theory[9] in a form of the Hubbard-I approximation (HIA)[10] has been applied to the elemental RE, and is shown to be superior to the DFT+U and semiempirical ligand field (or equivalently crystal field) theory[11]. It opens new opportunities to treat the electronic structure of complex materials containing RE elements.

Here, we report the charge self-consistent electronic structure theory of Ho@Pt performed by combining DFT with the exact diagonalization (ED)[12] of a single-impurity Anderson model[13]. In this approach, the DFT electronic structure obtained by the relativistic version[14,15] (with the spin-orbit coupling (SOC) included) of the full-potential linearized augmented plane wave method (FP-LAPW)[16] is consistently extended to account for the full structure of the 4*f*-orbital atomic multiplets and their interaction with the conduction bands[17]. Previously, the method was used to treat the 4*f*-electron materials in paramagnetic phase[8,18], and we extend it to the spin-polarized case.

[1]Institute of Physics, Czech Academy of Sciences, Na Slovance 2, CZ-18221, Prague, Czech Republic. [2]V. A. Kotel'nikov Institute of Radio Engineering and Electronics, Russian Academy of Sciences, Moscow, 125009, Russia. [3]Moscow Institute of Physics and Technology, Dolgoprudny, Moscow Region, 141700, Russia. [4]University of Hamburg, Jungiusstrasse 9, 20355, Hamburg, Germany. Correspondence and requests for materials should be addressed to A.B.S. (email: shick@fzu.cz)

	$\langle M_S\rangle$	$\langle M_L\rangle$	$\langle M_S\rangle+\langle M_D\rangle$	$\langle J_z\rangle$
DFT+U[1]	4.1	5.6	—	7.65
DFT+U[3]	3.91	5.88	—	7.84
$\Delta_{ex}=5$ meV	3.39	4.92	4.09	6.62
$\Delta_{ex}=10$ meV	3.32	5.14	4.28	6.80
$\Delta_{ex}=15$ meV	3.32	5.15	4.30	6.82
XMCD[2]	2.28 ± 0.12	4.28 ± 0.06	2.84 ± 0.13	5.42 ± 0.08

Table 1. Spin (M_S), orbital (M_L), M_S plus magnetic dipole M_D moments (in μ_B), and the total $\langle J_z\rangle = M_S/2 + M_L$ for the *fcc*-Ho adatom on Pt(111) with different values of the exchange splitting Δ_{ex}, in comparison with DFT+U[1,3] and experimental data[2].

Methodology

We use the $3\times3\times1$ supercell model with twenty seven Pt atoms (three layers), and the rare-earth adatom which is placed either in the *hcp*(-Ho@Pt) or the *fcc*(-Ho@Pt) hollow positions atop the Pt(111) surface (see supplemental Fig. S1). The symmetry of both adsorption sites is C_{3v}. The difference between *hcp*-Ho@Pt and *fcc*-Ho@Pt originates from the different placement of the Pt atoms in the sub-surface layer. The optimal heights for the rare-earth Ho adatoms above the Pt surface layer are taken from ref. 1 as $h_{hcp}=4.386$ bohr and $h_{fcc}=4.348$ bohr.

In the RE atoms the 4*f* electrons are mainly responsible for the magnetic moment, and the external *spd* electrons make only a discreet contribution to it. Their role, however, can not be disregarded, since these outer electrons strongly infuence the electronic and magnetic properties of the system. Therefore, we consider the multi-orbital Hamiltonian[10] $H=H^0+H^{\text{int}}$. H^0 is the one-particle Hamiltonian found from *ab initio* electronic structure calculations of a supercell; H^{int} is the on-site Coulomb interaction[10] describing the *f*-electron correlation. We assume that electron interactions in the *s*, *p*, and *d* shells are well approximated in DFT.

The DFT+ED calculations are performed in the charge self-consistent implementation described in section "Theoretical methods and computational details". The effects of the interaction Hamiltonian H^{int} on the electronic structure are accounted by a one-particle selfenergy Σ, which is constructed with the aid of an auxiliary impurity model Eq. (1) describing the complete seven-orbital 4*f* shell. The band Lanczos method[12] is employed to find the lowest-lying eigenstates of the many-body Hamiltonian H_{imp} and to calculate the one-particle Green's function G_{imp} and the selfenergy Σ in the subspace of the localized *f* orbitals $\{\phi_\gamma\}$ at low temperature ($k_BT=1/500$ eV). The Coulomb U values of 7.03 eV, and the exchange J of 0.83 eV were used, which are in the ballpark of commonly accepted values of U and J for the rare earths[19,20].

Results

The XMCD measurements[2] are performed in an external magnetic field (up to 7 T) assuming the magnetic saturation of the Ho@Pt system. Therefore, we have performed the spin-polarized calculations assuming the magnetic saturation of the Ho-adatom *f*-shell. In these calculations, we applied HIA and ED to DFT with the non-spin-polarized exchange-correlation functional[21] in order to exclude the contribution of *f*-intraorbital exchange field into the double-counting W_{dc}[22]. The exchange splitting Δ_{ex} in Eq. (1), which corresponds to the interorbital exchange energy between the 4*f* and 5*d* states of Ho, was varied as a parameter in a range from 5 meV to 15 meV (see the section "Theoretical methods and computational details" for further explanation of the Δ_{ex} choice). We have examined that it is enough to produce a fully spin-polarized solution and the selfenergy in Eq. (1).

First, we discuss the spin-polarized DFT+ED for the *fcc*-Ho@Pt. The *f*-states occupation $\langle n_f\rangle$ changes only a little - from 10.17 to 10.16 - with the change of Δ_{ex}. The calculated ground state magnetic properties are shown in Table 1 in comparison with the XMCD[2] experiments. The values of spin moment $M_S = -2\langle S_z\rangle\mu_B/\hbar$ change only a little with the change of Δ_{ex}. The changes in orbital moment $M_L = -\langle L_z\rangle\mu_B/\hbar$, and the magnetic dipole moment $M_D = -6\langle T_z\rangle\mu_B/\hbar$ are somewhat bigger indicating enhancement of the orbital polarization with an increase of Δ_{ex}. Due to simultaneous increase of the orbital M_L and the the magnetic dipole M_D moments, the ratio $R_{LS} = \frac{M_L}{M_S+M_D} = 1.20$ does not change with an increase of Δ_{ex}. It is somewhat smaller than the XMCD result[2] R_{LS} 1.51 ± 0.09, but still in reasonable agreement with the experiment. The magnitude of the total moment $\langle J_z\rangle = M_S/2 + M_L$ of 6.6 ($\Delta_{ex}=5$ meV), and 6.8 (10–15 meV) exceeds somewhat the experimental $\langle J_z\rangle$ of 5.34–5.50[2]. It is closer to $\langle J_z\rangle=6$[2] obtained in the multiplet calculations than to $\langle J_z\rangle=8$[1] inferred from DFT+U. Note that in the presence of the crystal-field interaction, the values of the magnetic moment $M_J=M_S+M_L$ obtained from the data of Table 1 are smaller than the maximum magnetic moment $g_JJ=9.84$, where $g_J=1.23$ is the Lande factor and $J=8.00$ is the expectation value of the total moment calculated for the ground state of Eq. (1). No noticeable differences are found for Ho@Pt in *fcc* and *hcp* positions (see supplemental Table S2).

The total and $j=5/2$, $7/2$ projected *f* orbital density of states (fDOS) for the spin-polarized *fcc*-Ho@Pt and $\Delta_{ex}=10$ meV is shown in Fig. 1(A). DFT+ED yields for the occupied 4*f*-states the first multiplet peak at ~4 eV below E_F, and for the empty states at ~2.5 eV, consistent with the bulk hcp-Ho PES[23]. Effect of spin-polarization is illlustrated in Fig. 1(B) where the spin-resolved fDOS is shown. The spin-↑ intensities lie at ~7–8 eV below E_F, and the spin-↓ at ~4–6 eV below E_F. The empty states of spectrum at ~2–4 eV are practically fully spin-polarized. There is no surprise that these states are dominated by the $j=7/2$ contribution since the $j=5/2$ states are fully occupied for the f^{10} manifold.

The energy splitting of the seventeen lowest many-body eigenvalues of Eq. (1), which correspond to the expectation value of $J_f=8.00$, are shown in Fig. 2(A) (also see supplemental Table S3). The lowest energy is

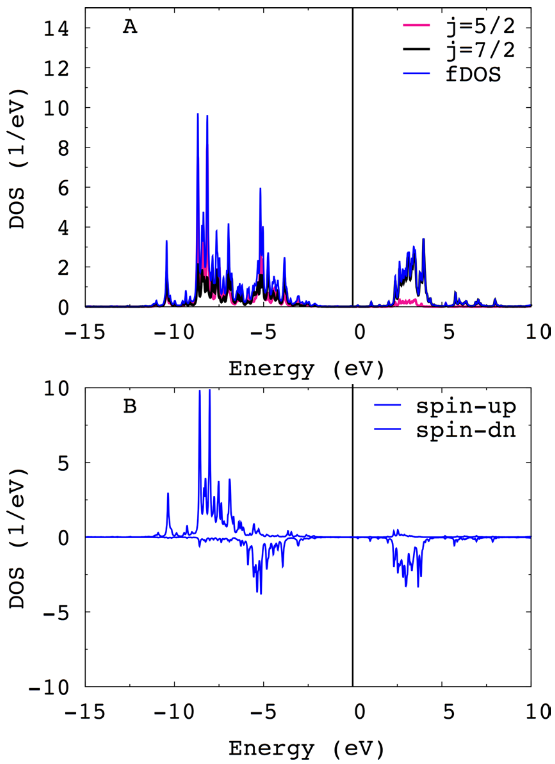

Figure 1. The total and $j = 5/2$, $7/2$ projected fDOS for the fcc-Ho@Pt(111) (**A**); the spin projected fDOS for the fcc-Ho@Pt(111) (**B**).

$|J = 8, J_z = 7.00\rangle$ state, next to it is the state $|J = 8, J_z = 5.98\rangle$ which is 10 meV higher in the energy, and the third state is $|J = 8, J_z = 0.02\rangle$, higher in the energy by 6 meV. This energy difference determines the magnetic anisotropy energy (MAE) barrier of 16 meV to turn the magnetization from the out-of-plane to the in-plane orientation. This value is about three times smaller than the MAE obtained by DFT+U[1].

The experimental IETS results[1] yield the spin excitations at the 5 meV and 8 meV energies. However, in the further experiments[3], no signature of inelastic signal distinguishable from the substrate spectrum was found. We have calculated the model IETS spectra for the polarized *fcc*-Ho@Pt as given in the Supplemental material. We found shallow steps at the low energies ±10 meV, and other steps at the energies over 40 meV. Thus, our results disagree with earlier experiments of Miyamachi *et al.*[1]. Whether the calculated steps can be seen in the experiments depends on the intensity of the differential conductance (see the Eq. (S3) in Supplemental Material). Since it is proportional to the very small hybridization strength ~17 meV, the IETS intensity will be further reduced. We conclude that our results do not contradict qualitatively the experimental findings[3].

Once the magnetic field is switched off, the adatom becomes non-magnetic. The self-consistent solution of Eq. (3) for paramagnetic state ($\Delta_{ex} = 0$) represents the final state after the demagnetization. In this state, the *f*-electron count $\langle n_f \rangle$ changes to 10.5, and the crystal field changes as well (see supplemental Table S4 for comparison between spin-polarized and paramagnetic Δ_{CF}). It is not surprising, since the symmetry of the many-body ground state of Eq. (1) is changing, inducing the changes in the local occupation matrix $n_{\gamma_1\gamma_2}$ and corresponding effective LDA+U potential V_U in Eq. (3). This effect is neglected in semiempirical ligand field theory.

The energy splitting of the seventeen lowest many-body eigenvalues of Eq. (1) in paramagnetic state are shown in Fig. 2(C)) (also see supplementary Table S3). The lowest energy is the $|J = 8, J_z = \pm 7.95\rangle$ state, in agreement with $\langle J_z \rangle = \pm 8$[1]. Next to it is the state $|J = 8, J_z = \pm 5.36\rangle$ which is 6.5 meV higher in the energy, and the second exited state is $|J = 8, J_z = 0.0\rangle$, higher in the energy by 1.4 meV. This energy difference determines the so-called zero-field splitting energy barrier of 7.9 meV, which is twice as large as given by the ligand field theory[2]. Note, that application of the external magnetic field of 7 T to this paramagnetic state in Eq. (1) will not produce the spin-polarized solution shown in Fig. 2(A), since the parameters of the Eq. (1) hamiltonian are different (Δ_{CF}, Δ_{ex}, e_f). This difference is determined by the charge self-consistency, and the 5*d*–4*f* interorbital exchange coupling. This spin-polarized ground state can not be described by simple re-population of the Zeeman-split non-magnetic many-body levels.

The transition from the initial magnetically polarized state to the final paramagnetic state in the quantum regime is a complex problem[24] and we leave the theoretical description of the magnetization dynamics for future considerations. Nonetheless, we notice that if we assume $\Delta_{ex} = 0$ while keeping all other parameters in Eq. (1) the same as in the spin-polarized case, the ground state changes to $|J = 8, J_z = 0\rangle$ and the adatom becomes magnetically unstable (see Supplemental Material).

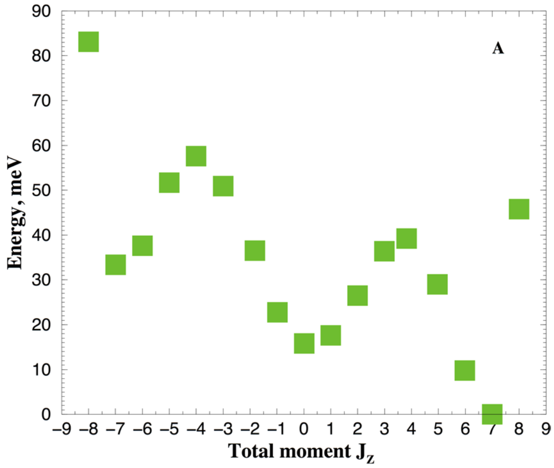

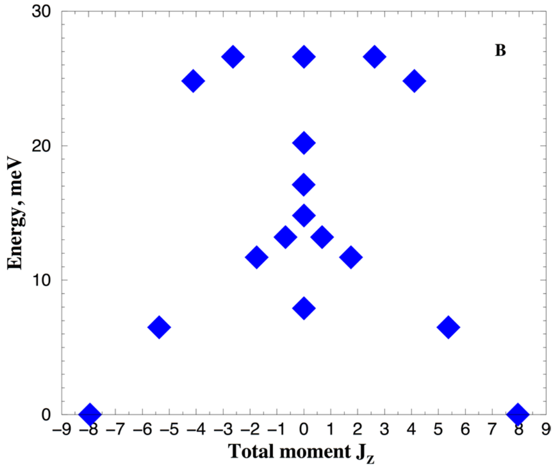

Figure 2. Scheme of quantum many-body levels of the lowest $J_f = 8.00$ multiplet obtained in Eq. (1) with the Δ_{CF} parameters for spin-polarized calculations and $\Delta_{ex} = 10$ meV (**A**); with the Δ_{CF} parameters for non-spin-polarized calculations (**B**).

Conclusions

To summarize, comparison between spin-polarized and paramagnetic DFT+ED solutions for Ho@Pt shows that the correct 4*f* magnetic state in the presence of the external magnetic field can not be correctly described by simple re-population of the Zeeman-split many-body levels of a non-magnetic semiempirical hamiltonian. It is due to non-negligible role of the interaction between 4*f* and 5*d* electrons. We emphasize the role of 5*d*–4*f* interorbital exchange polarization in modification of the 4*f* shell energy spectrum, and overrule the existence of the magnetic $\langle J_z \rangle = 8$ ground state[1].

Theoretical Method and Computational Details

The multi-orbital impurity solver includes the full spherically symmetric Coulomb interaction, the spin-orbit coupling (SOC), the crystal field term (CF) describing the Coulomb interaction of the *f*-shell with other electrons, and the inter-orbital exchange field acting on the *f*-shell from other electrons. The corresponding Hamiltonian can be written as ref. 13

$$\begin{aligned} H_{\text{imp}} &= \sum_{\substack{kmm' \\ \sigma\sigma'}} [\epsilon^k]_{mm'}^{\sigma\,\sigma'} b_{km\sigma}^\dagger b_{km'\sigma'} + \sum_{m\sigma} \epsilon_f f_{m\sigma}^\dagger f_{m\sigma} \\ &+ \sum_{mm'\sigma\sigma'} [\xi \mathbf{l}\cdot\mathbf{s} + \Delta_{\text{CF}} + \Delta_{\text{ex}} s_z]_{mm'}^{\sigma\,\sigma'} f_{m\sigma}^\dagger f_{m'\sigma'} \\ &+ \sum_{\substack{kmm' \\ \sigma\sigma'}} ([V^k]_{mm'}^{\sigma\,\sigma'} f_{m\sigma}^\dagger b_{km'\sigma'} + \text{h. c.}) \\ &+ \frac{1}{2} \sum_{\substack{mm'm'' \\ m'''\sigma\sigma'}} U_{mm'm''m'''} f_{m\sigma}^\dagger f_{m'\sigma'}^\dagger f_{m'''\sigma'} f_{m''\sigma'}, \end{aligned} \tag{1}$$

where $f^{\dagger}_{m\sigma}$ creates an electron in the 4*f* shell and $b^{\dagger}_{m\sigma}$ creates an electron in the "bath" that consists of those host-band states that hybridize with the impurity 4*f* shell. The energy position ϵ_f of the impurity level, and the bath energies ϵ^k are measured from the chemical potential μ. The parameters ξ, $\Delta_{\rm ex}$, and matrix $\Delta_{\rm CF}$ specify the strength of the SOC, the exchange field, and the size of CF, acting on the *f*-shell. The parameter matrices V^k describe the hybridization between the 4*f* states and the bath orbitals at energy ϵ^k. The bath parameters V^k and ϵ^k are determined from the LDA Green function $G_{\rm LDA}(z)$ as described in ref. 18, and are shown in supplemental Table S1. The Ho *f*-shell SOC parameter $\xi = 0.28$ eV in Eq. (1) was determined from LDA calculations.

The exchange splitting $\Delta_{\rm ex}$ in Eq. (1) corresponds to the interorbital exchange energy between the 4*f* and mainly 5*d* states of Ho, $J_{\rm fd} m_{5d}$[22], where $J_{\rm fd}$ is ~0.1 eV[25], and m_{5d} is the magnetic moment of the 5*d* states. As follows from the DFT and DFT+U calculations[3] as well as from our own calculations, the m_{5d} does not exceed 0.1 μ_B. It sets $\Delta_{\rm ex} = 10$ meV as an energy scale for the $J_{\rm fd} m_{5d}$. Note that $\Delta_{\rm ex}$ exceeds the maximum external magnetic field value (0.4 meV) used in the XMCD experiments by an order of magnitude, and we did not include this field in the calculations.

The many-body Hamiltonian $H_{\rm imp}$ is solved employing the band Lanczos method[12] and the selfenergy is obtained. The local Green's function $G(z)$ in the subspace of the localized spinorbitals $\{\phi_\gamma, \gamma = (lm\sigma)\}$, defining the *f* manifold of the rare-earth adatom, is calculated[17] as

$$G(z) = [G_0^{-1}(z) + \Delta\epsilon_\sigma - \Sigma(z)]^{-1}, \tag{2}$$

where $G_0(z)$ is the non-interacting Green's function, and $\Delta\epsilon_\sigma$ are chosen to ensure the n_f^σ occupations equal to the given number of spin-↑,↓ correlated electrons. The matrix $n_{\gamma_1\gamma_2} = -\frac{1}{\pi}{\rm Im}\int_{-\infty}^{E_{\rm F}} {\rm d}z\,[G(z)]_{\gamma_1\gamma_2}$ is used to construct an effective LDA+*U* potential V_U, which is inserted into Kohn–Sham-like equations:

$$[-\nabla^2 + V_{\rm LDA}(\mathbf{r}) + V_U + \xi(\mathbf{l}\cdot\mathbf{s})]\,\Phi^b_{\mathbf{k}}(\mathbf{r}) = \epsilon^b_{\mathbf{k}}\Phi^b_{\mathbf{k}}(\mathbf{r}). \tag{3}$$

Note that the DFT contributions to the effective potential $V_{\rm LDA}$ in Eq. (3) are corrected to exclude the double-counting of the *f*-states non-spherical contributions to the DFT and DFT+U parts of the potential[17].

These equations are iteratively solved until self-consistency over the charge density is reached. In each iteration, a new Green's function $G_0(z)$, and a new value of the 4*f*-shell occupation are obtained from the solution of Eq. (3). Subsequently, a new selfenergy $\Sigma(z)$ corresponding to the updated 4*f*-shell occupation is constructed. Finally, the next iteration is started by evaluating the new local Green's function, Eq. (2). The self-consistent procedure defined by Eqs 1–3 was repeated until the convergence of the 4*f*-manifold occupations $n_f^{\uparrow,\downarrow}$ was better than 0.01.

The CF matrix $\Delta_{\rm CF}$ in Eq. (1) is obtained by projecting the solutions of Eq. (3) into the $\{\phi_\gamma\}$ local *f*-shell basis,

$$[H]_{\gamma_1\gamma_2} = \int_{-\infty}^{+\infty} {\rm d}\epsilon\epsilon[N(\epsilon)]_{\gamma_1\gamma_2}, \tag{4}$$

where, $[N(\epsilon)]_{\gamma_1\gamma_2}$ is an f-projected density of states (fDOS) matrix. The matrix elements of Δ_{CF} are then obtained by removing the interacting LDA+*U* potential $[V_U]_{\gamma_1\gamma_2}$ and SOC $[\xi\mathbf{l}\cdot\mathbf{s}]_{\gamma_1\gamma_2}$ from the local hamiltonian Eq. (4).

Since some electron-electron interaction energy is already included in LDA, the potential V_U in Eq. (3) includes the so-called double-counting correction $W_{\rm dc}$. Due to a self-consistency condition $\epsilon_f = -W_{dc}$[17], it determines the mean position of the interacting *f*-level in Eq. (1), and controls the number of *f*-electrons. For the bulk Ho, the positions and the spectral shape of the occupied 4*f*-states are in a reasonable agreement with experimental valence-band photoelectron spectroscopy (PES)[23], when the "around-mean-field" (AMF)[6] flavour for $W_{\rm dc}$ is used (see Supplemental Material). Therefore, we used this $W_{\rm dc}$ in the Ho@Pt calculations.

References

1. Miyamachi, J. H. *et al*. Stabilizing the magnetic moment of single holmium atoms by symmetry. *Nature* **503**, 242 (2013).
2. Donati, F. *et al*. Magnetism of Ho and Er Atoms on Close-Packed Metal Surfaces. *Phys. Rev. Lett.* **113**, 237201 (2014).
3. Steinbrecher, M. *et al*. Absence of a spin-signature from a single Ho adatom as probed by spin-sensitive tunneling. *Nature Communications* **7**, 10454 (2016).
4. Donati, F. *et al*. Magnetic remanence in single atoms. *Science* **352**, 318 (2016).
5. Karbowiak, M. & Rudowicz, C. Ground state of Ho atoms on Pt(111) metal surfaces: Implications for magnetism. *Phys. Rev. B* **93**, 184415 (2016).
6. Anisimov, V. I., Zaanen, J. & Andersen, O. K. Band theory and Mott insulators: Hubbard U instead of Stoner I. *Phys. Rev. B* **44**, 943 (1991).
7. Lichtenstein, A., Anisimov, V. I. & Zaanen, J. Density-functional theory and strong interactions: Orbital ordering in Mott-Hubbard insulators. *Phys. Rev. B* **52**, R5467(R) (1995).
8. Kozub, A. *et al*. Electronic structure and magnetism of samarium and neodymium adatoms on free-standing graphene. *Phys. Rev. B* **94**, 125113 (2016).
9. Georges, A., Kotliar, G., Krauth, W. & Rozenberg, M. Dynamical mean-field theory of strongly correlated fermion systems and the limit of infinite dimensions. *Rev. Mod. Phys.* **68**, 13 (1996).
10. Lichtenstein, A. I. & Katsnelson, M. I. Ab initio calculations of quasiparticle band structure in correlated systems: LDA++ approach. *Phys. Rev. B* **57**, 6884 (1998).
11. Locht, I. L. M. *et al*. Standard model of the rare earths analyzed from the Hubbard I approximation. *Phys. Rev. B* **94**, 085137 (2016).
12. Kolorenc, J., Poteryaev, A. & Lichtenstein, A. I. Valence-band satellite in ferromagnetic nickel: LDA+DMFT study with exact diagonalization. *Phys. Rev. B* **85**, 235136 (2012).
13. Hewson, A. *The Kondo Problem to Heavy Fermions* (Cambridge University Press, 1993).
14. Shick, A. B., Liechtenstein, A. I. & Pickett, W. E. Implementation of the LDA+U method using the full-potential linearized augmented plane-wave basis. *Phys. Rev. B* **60**, 10763 (1999).

15. Shick, A. B. & Pickett, W. E. Magnetism, spin-orbit coupling, and superconducting pairing in UGe_2. *Phys. Rev. Lett.* **86**, 300–303 (2001).
16. Wimmer, E., Krakauer, H., Weinert, M. & Freeman, A. J. Full-potential self-consistent linearized-augmented-plane-wave method for calculating the electronic structure of molecules and surfaces: O_2 molecule. *Phys. Rev. B.* **24**, 864 (1981).
17. Shick, A. B., Kolorenc, J., Lichtenstein, A. I. & Havela, L. Electronic structure and spectral properties of Am, Cm, and Bk: Charge-density self-consistent LDA+HIA calculations in the FP-LAPW basis. *Phys. Rev. B* **80**, 085106 (2009).
18. Shick, A. B., Havela, L., Lichtenstein, A. I., Katsnelson, M. I. & Caciuffo, R. Racah materials: role of atomic multiplets in intermediate valence systems. *Nature Scientific Reports* **5**, 15429 (2015).
19. van der Marel, D. & Sawatzsky, G. Electron-electron interaction and localization in d and f transition metals. *Phys. Rev. B* **37**, 10674 (1988).
20. Lebegue, S. *et al.* Multiplet effects in the electronic structure of light rare-earth metals. *Phys. Rev. B* **74**, 045114 (2006).
21. Shorikov, A. O., Lukoyanov, A. V., Korotin, M. A. & Anisimov, V. I. Magnetic state and electronic structure of the δ and α phases of metallic Pu and its compounds. *Phys. Rev. B* **72**, 024458 (2005).
22. Peters, L. *et al.* Treatment of 4f states of the rare earths: The case study of TbN. *Phys. Rev. B* **89**, 205109 (2014).
23. Lang, S., Baer, Y. & Cox, P. Study of the 4f and valence band density of states in rare-earth metals. II. Experiment and results. *J. Phys. F: Met. Phys.* **11**, 121 (1981).
24. Karlewski, C. *et al.* Magnetic adatoms as memory bits: A quantum master equation analysis. *Phys. Rev. B* **91**, 245430 (2016).
25. Brooks, M., Eriksson, O. & Johansson, B. 3d–5d band magnetism in rare earth transition metal intermetallics: $LuFe_2$. *J. Phys. Condens. Matter* **1**, 5861 (1989).

Acknowledgements

We acknowledge stimulating discussions with P. Jelínek, and H. Brune. Financial support was provided by the Czech Science Foundation (GACR) grant No. 15-05872J, the Deutsche Forschungsgemeinschaft (DFG) Grant No. DFG LI 1413/8-1. D.S.S. acknowledges financial support from Russian Foundation of Basic Research (project No. 15-02-02128), the Fellowship of the President of Russian Federation for young scientists (fellowship No. SP-2044.2016.5), and the Ministry of Education and Science of the Russian Federation (grant No. 14.Y26.31.0007). Access to computing and storage facilities owned by parties and projects contributing to the National Grid Infrastructure MetaCentrum provided under the programme "Projects of Large Research, Development, and Innovations Infrastructures" (CESNET LM2015042), is appreciated.

Author Contributions

A.B.S., D.S.S. and A.I.L. conceived and supervised the project. A.B.S. and D.S.S. performed the computations. All authors contributed to the interpretation of the data and to the writing of the manuscript.

Additional Information

Supplementary information accompanies this paper at doi:10.1038/s41598-017-02809-7

Competing Interests: The authors declare that they have no competing interests.

Publisher's note: Springer Nature remains neutral with regard to jurisdictional claims in published maps and institutional affiliations.